Multibeam echosounder backscatter strength signature of dune fields in the Belgian part of the north Sea.

M. Roche *Federal Public Service Economy, Continental Shelf Service, 1000 Brussels*
F. Barette *Federal Public Service Economy, Continental Shelf Service, 1000 Brussels*
K. Degrendele *Federal Public Service Economy, Continental Shelf Service, 1000 Brussels*
A.-S. Piette *Federal Public Service Economy, Continental Shelf Service, 1000 Brussels*

ABSTRACT: The relationship between asymmetrical sand waves morphology, surface sediment and multibeam backscatter is investigated by analysing three sand waves fields located on different sandbanks in the Belgian part of the North Sea. High resolution multibeam bathymetric and backscatter data, Van Veen grab samples and sediment profile imaging data were acquired specifically for this study in October 2022. Special care was taken to ensure accurate positioning of sediment samples and seafloor images to allow reliable correlation with acoustic data and assignment of each sample to a sand wave morphological unit (stoss side, crest, lee side and trough). Grain size analysis of the fraction above 2 mm completes the data set. Overall, the variation in backscatter levels is in line with the dune morphology, but shifts are observed locally. The highest backscatter values are detected along the stoss sides and on the crests. A significant positive correlation is observed between backscatter and the percentage of gravel composed mainly of shell fragments. The highest correlations correspond to grain classes close to the wavelength of the acoustic signal. In the northern area, a particular multi-crests sand waves morphology is observed likely to be related to the antagonism of ebb and flow and the particular nature of the sediment, half of which consisting of shells and shell fragments ranging from 2 mm to 8 mm.

1 INTRODUCTION

The sorting of surface sediments across tidal sand waves shows that, in general, coarser grains tend to accumulate on the stoss sides and crests while finer sediments are concentrated on the lee sides and troughs (Van Lancker and Jacobs, 2000; Cheng et al., 2020; Gaida et al., 2020). Modeling studies largely confirm this pattern (Roos et al., 2007; Damveld at al., 2020). However, reverse trends are also mentioned (Wemmenhove, 2004; Anthony and Leth, 2002). These antagonisms could be related to differences in hydrodynamics and sediment composition (Van Oyen and Blondeaux, 2009).

Multibeam echosounder (MBES) technology, which simultaneously records bathymetry and backscatter (BS), is a particularly well suited tool for the mapping of sand waves with a high spatial resolution. The high resolution bathymetric data allows the calculation of appropriate angular and insonified area corrections to be applied to the raw BS measurements. Once corrected, the BS is an excellent proxy for the sediment, as well as, if calibrated, comparable from one MBES to another, as long as the measurements are taken in the same frequency range (Lurton and Lamarche, 2015).

This paper presents a series of MBES measurements controlled by Van Veen grab samples and Sediment Profile Imaging (SPI) on three areas locates on the Belgian part of the North Sea and shaped by sand waves. The aim is to analyse, compare and evaluate the relationships between surface sediments and sand wave morphology. Some critical methodological issues are also highlighted.

2 MATERIAL AND METHODS

2.1 Study areas

The three study areas are located on different sandbanks in the Belgian part of the North Sea (Figure 1).

The southernmost BR area is located north of the Buiten Ratel, on the northern edge of a depression that divides the bank into two sides in its northern central part. Deep from -14.8 to -20.7 m Lower Astronomical Tide (LAT), BR area covers 13.7 ha (670 m by 205 m) and is modelled by sand waves oriented NW-SE with wavelengths of 200-250 m and amplitudes of 3-4 m (Figure 2a). In BR area the sand waves show a rather pronounced asymmetry $\left(\frac{L\ stoss\ side - L\ lee\ side}{L\ stoss\ side + L\ lee\ side}\right)$ with a mean value of 0.6 (Figure 2b). Bathymetric time series collected from 2010 to 2022 indicate an average migration speed of the sand waves of 2.7 m/year to the north-east. This displacement is lower than the displacement values given for sand waves of similar asymmetry (Knaapen, 2005). A cumulative volume of 143 10^3 m^3 of sand was removed from this area mainly from 2003 to 2014. Since then, this part of the sandbank has been closed to sand extraction.

Located in the western part of the Thornton sandbank, TB area occupies a seabed surface of 9.5 ha (533 m by 179 m) with depths ranging from -20.3 to -25.5 m LAT. The sand waves modelling this area are oriented NW-SE with wavelengths around 150 m and amplitudes of 4 m (Figure 3a). These sand waves are substantially asymmetric with a mean value of 0.4 (Figure 3b). For these sand waves, an average migration speed of 2.6 m/year towards the NE has been estimated on time series of bathymetric measurements made from 2014 to 2022. As for BR area, this displacement is lower than the values published by Knaapen (2005) for sand waves of similar asymmetry. Overall, these sand waves are morphologically very similar to those of the BR area. TB area was subject to fairly intensive sand extraction between 2014 and 2020 with a cumulative extracted volume of 221 10^3 m^3. Since 2021, extraction is prohibited in this area.

The WH area is located at the northern extent of the Westhinder sand bank. This area covers 18.3 ha (870 m by 210 m) with depths ranging from -10.8 to -28.5 m LAT. Giant sand waves curving westwards at the northern end of the Westhinder bank are oriented NW-SE in the WH area. These sand waves have variable wavelengths ranging from 240 to 320 m and variable amplitudes from 5 to 11 m (Figure 4a). These sand waves show asymmetries with values of about 0.4 in opposite directions: eastward for the sand wave located at the west of WH and westward for the two sand waves located at the centre and east of WH. The comparison of the current morpho-bathymetric situation with those of 2009 and 2013 demonstrates an average migration rate of 0.6 m/yr in the two opposite directions in agreement with the asymmetry orientation.

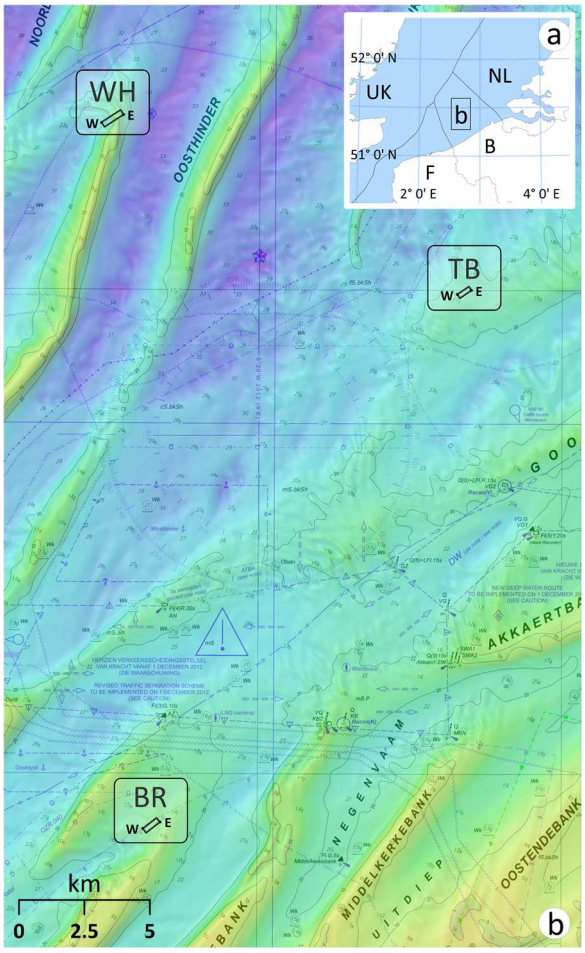

Figure 1. a: Regional location of the surveyed areas. b: Detailed location of the surveyed areas in the Belgian part of the North Sea. BR area, northern part of the Buiten Ratel sandbank (W: 51° 18.8550', 2°

36.2477'; E: 51° 18.9914', 2° 36.8075'); TB area, western part of the Thorntonbank (W: 51° 29.9222', 2° 46.5438'; E: 51° 30.0038', 2° 47. 0116'); WH area, northern end of the Westhinder bank (W: 51° 33.4358', 2° 34.7586'; E: 51° 33.5969', 2° 35.4870'); latitude and longitude in WGS84 degree decimal minutes; base map: Hydrographic map BNZ 2014 from Flemish Hydrographic Service combined with Bathymetric terrain model LAT from Flemish Hydrographic Service and FPS Economy.

2.2 MBES data

Bathymetric and backscatter (BS) data were collected using a Kongsberg EM2040 MKII 04 Dual Rx multibeam echosounder (MBES) installed on the RV Simon Stevin. This system is coupled with an IX Blue Octans motion sensor and an MGB-Tech RTK GPS positioning system, together ensuring decimetric XYZ accuracy of the data. A SBE 21 SeaCAT thermosalinograph provides continuous sound velocity measurements. To ensure inter-comparability of BS levels, all MBES data were recorded using the same acquisition settings (300 kHz, normal multi-sector transmission mode, medium pulse length of 108 µs).

The bathymetric data were processed following a standard workflow with QPS-Qimera® (2.5.1, 2022): integration of the RTK correction, reduction of the Z values in the LAT, fine-tuning of the roll, pitch and heading offsets and cleaning of the soundings. Finally, a bathymetric model with a resolution of 1x1 m was calculated for each of the study areas.

BS data were processed using QPS-FMGT® (7.10.2, 2022). The previously calculated bathymetric model has been incorporated to refine the estimation of incidence angles and insonified areas. The beam pattern has been corrected for. For cartographic purposes, a continuous BS mosaic with a resolution of 1x1 m is calculated with all the BS values.

However, only BS data acquired in the range of incidence angles ±[20°,60°] are considered to ensure a rigorous spatial inter-comparability of the BS values and analysis of the correlations with sand wave morphological units and sediment granulometry.

Limiting the use of BS to this angular range has a double advantage: within it, the BS values are stable regarding the incident angle and, as they are essentially controlled by the impedance contrast, the roughness and the volume scattering of the sediment, they are the ones that best discriminate sediment types. (Jackson et al., 1986; APL, 1994; Lamarche and Lurton, 2018).

2.3 Ground truthing

For each area, a series of Van Veen grab samples and Sediment Profile Imaging (SPI) images were taken along a transect perpendicular to the sand wave crests immediately after the acoustic measurements (17 for BR, 13 for TB and 4 for WH). The grab samples and SPI images are not strictly in the same position: the Van Veen was operated with the starboard winch of the RV Simon Stevin, the aft winch was used for the SPI. The raw positions of the grab samples and SPI images were carefully corrected for the respective distances of the two winches from the GPS antenna and for the ship's heading at the moment the instruments touched the seabed. These corrections are essential to ensure a correct spatial match between the sedimentological and acoustic data. The corrected positions of the grab samples and SPI images are shown by area on the bathymetric and BS maps in Figures 2, 3 and 4.

After drying the samples, a particle size analysis of the fraction larger than 2 mm was carried out by weighing, using 2, 4, 8, 16 and 32 mm sieves. Observation of the sediments shows that the gravelly fraction mainly consists of whole shells and shells fragments. The analysis of the sandy fraction of less than 2 mm in size is carried out using a Malvern Mastersizer 3000 laser particle analyser. Semi-quantitatively, 4 classes of shell density at the sediment surface were estimated from

the raw SPI images (0 = absent, 1 = present, 2 = abundant, 3 = very abundant).

3 ANALYSIS AND RESULTS

The analyses were carried out at two scales. Locally, in each of the areas, profiles combining bathymetry and BS in the incidence angle interval of ±[20°, 60°] make it possible to assess the spatial relationship between the morphology of the sand waves and the BS variations. Globally, in order to analyze the relationships between the level of BS, the morphology of the sand waves and the granulometry of the sediments, the descriptive statistics of BS (mean and std) in the angular interval ±[20°, 60°] were estimated in rectangles of 50x10 m around the samples. The orientation of the rectangles was defined by calculating the median value of the aspect (downward direction of the maximum rate of change in value from each cell to its neighbours) derived from the bathymetric model resampled to a 5x5 m resolution, within a buffer with a radius of 20 m around each sample location. This method ensures the calculation of BS statistics in homogeneous morphological units of sand waves surrounding the grab samples. Around the positions of the SPI images, BS statistics were extracted using the same principle. Depending on its position, each sample was assigned to a sand wave morphological unit (stoss side, crest, lee side and trough). Global correlations between all the variables considered were established using a summary table gathering all the data.

3.1 BR area

The data collected in the BR area are summarised in Fig. 2. The profile in fig. 2c shows a spatial correlation between the BS and the bathy-morphology. The highest BS values, around -14 dB, are observed on the stoss sides. In the lee troughs the BS values drop to -19 dB. Considering the ± 1 dB inherent transducer sensitivity reported for Kongsberg MBES systems (Hammerstad, 2000), the observed difference of 5 dB is definitely significant. The sediments on the stoss sides reflect three times more acoustic energy than those on the leeward troughs. However, the BS and bathymetric profiles show a phase shift for two of the three sand waves in the BR area. For these two sand waves, the BS level decreases progressively in the middle part of the stoss sides, so that their ridges have intermediate BS values around -17 dB. The third sand wave located in the eastern part of BR shows a perfect phasing between bathy-morphology and BS.

The grain size analysis of the grab samples demonstrates the predominantly sandy nature of the surface sediments in the BR area: the percentage of the sandy fraction ranges from 90% to practically 100% with an average of 97%. The gravelly fraction is composed mostly of shell fragments between 2 and 16 mm.

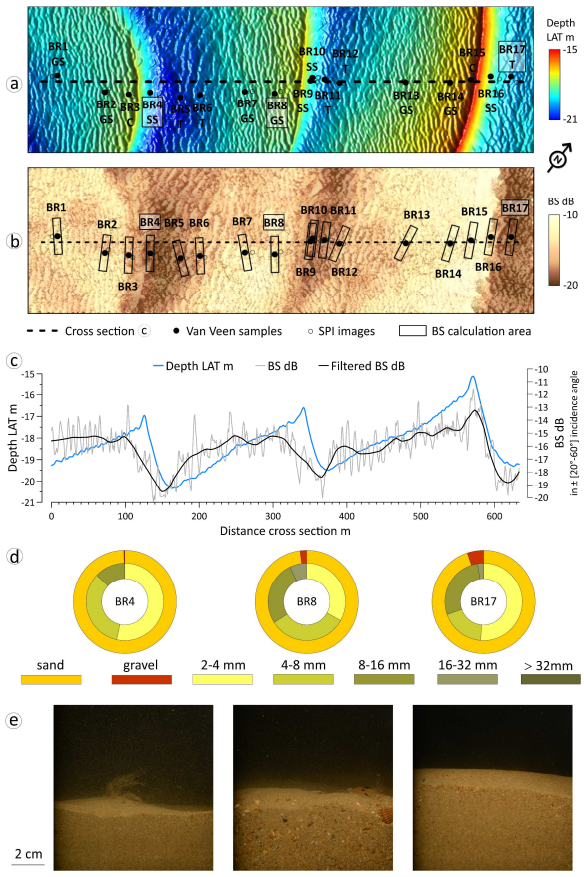

Figure 2. Summary of data collected over BR area. a: Bathy-morphological map (depth in LAT m) with positions of grab samples, SPI images and cross section presented in 2 c , XY scale is given by the cross section, assignment to a morphological unit is indicated below the sample ID (GS = stoss side - gentle slope, C = ridge - crest, SS = lee side - steep slope and T = trough); b: BS map (dB), positions of grab

samples, 50x10m buffers used for BS statistics calculation and c section; c: Bathymetry and BS cross-section (average of values over a 20 m corridor on either side of the line) (BS raw data and filtered data using a lowess Gaussian quadratic function); d: Granulometry of samples BR4, BR8 and BR9, outer ring gives the percentages of sand and gravel, inner ring gives the percentages of the gravel classes; e: SPI images of samples BR4, BR8 and BR9.

In agreement with the spatial correlation observed between the BS and the morphology of the sand waves, the highest percentages of gravel are observed in the gentle slope and ridge samples and, on the contrary, the lee side and through samples are overall very poor in gravel (fig. 2d). The observation of SPI images suggests a fairly homogeneous seafloor with few surface scatterers (fig. 2e).

3.2 TB area

Figure 3 summarises the data collected in TB area. The BS variations correlate very well with the bathymetric variations of the three sand waves (fig. 3c). The stoss and lee sides and the through show low BS quite stable values around -17 dB. On the stoss side, around -22.5 m LAT, the slope break marking a quick decrease in the bathymetry, is accompanied by an increase in the BS level up to the ridges, where the values reach -14 dB. Beyond the ridges, on the leeward side, the BS decreases in parallel with the bathymetry to return to values oscillating around -17 dB.

TB samples (fig. 3d) show a predominantly sandy grain size composition with the proportion of grains smaller than 2 mm ranging from 77 to 98% with an average of 89 %. The gravels are mainly composed of shell fragments between 2 and 16 mm. With the exception of one sample (TB03) situated on the leeward side, all samples with a gravel fraction greater than 10 % come from the sand wave crests. Here the relationship between the BS, the sediment and the morphology of the sand waves is clear.

The SPI images (fig. 3e) show a contrasting interface from sample to sample with a semi-quantitative estimate of the

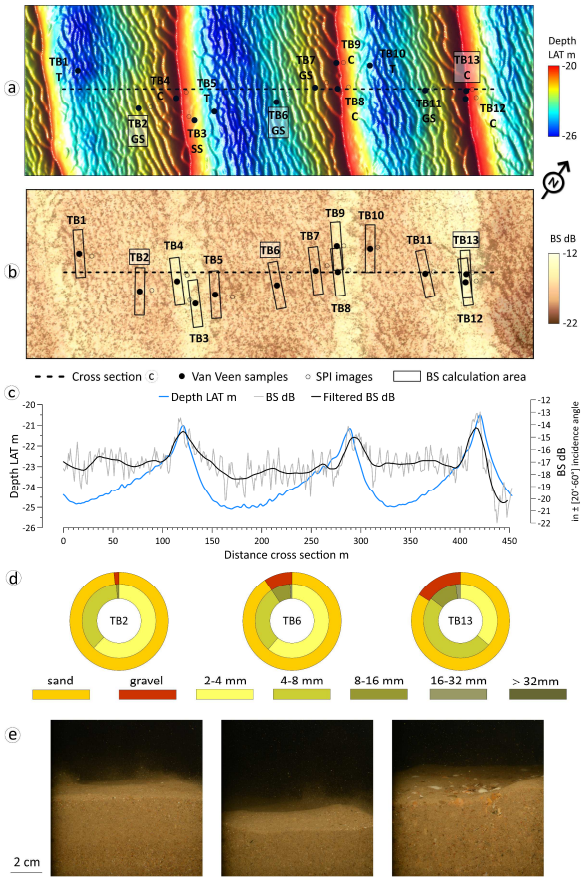

Figure 3. Summary of data collected over TB area. Refer to the legend of Figure 2 (only values, scales, grab samples labels and SPI images differ).

abundance of scatterers present on the sediment surface varying between absent and very abundant. However, no discernible relationship is observed between this semi-quantitative estimate of the abundance of scatterers present on the sediment surface with the BS and the particle size composition of the sediment.

3.3 WH area

Fig. 4 presents the data collected on the WH zone. In the WH area, due to the opposing asymmetry of the sand waves, their relationship with the BS has to be considered separately. The western sand wave, shows BS levels that follow the bathymetry with a phase shift, the BS level increasing from -14 to -10 dB from the middle part of the stoss side to the end of the lee side (fig. 4c). The BS-bathymetry phase shift is the opposite of that observed in the BR area.

In the eastern area, the BS fluctuates by 1 to 2 dB around -10 dB, which represents 4 to 5 times the acoustic energy reflected by the sands of BR and TB areas. These variations are not spatially related to the bathymetry. The particular type of sediment in this area explains the high BS values. The gravel fraction of the 3 samples taken in this part of WH ranged from 22% to 50%, with an average of 40% (fig. 4d). As can be seen from the composition of the grab samples and the SPI images, these gravels consist mainly of shells and shell fragments (fig. 4e). The sand waves in this area are made up of a sediment that consists of up to 50% of shell fragments with grain sizes between 2 and 8 mm.

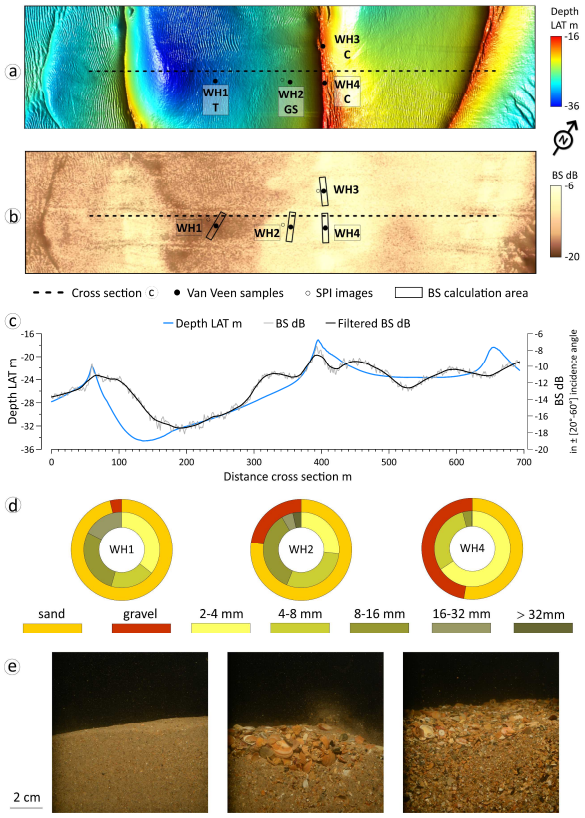

Figure 4. Summary of data collected over WH area. Refer to the legend of Figure 2 (only values, scales, grab samples labels and SPI images differ).

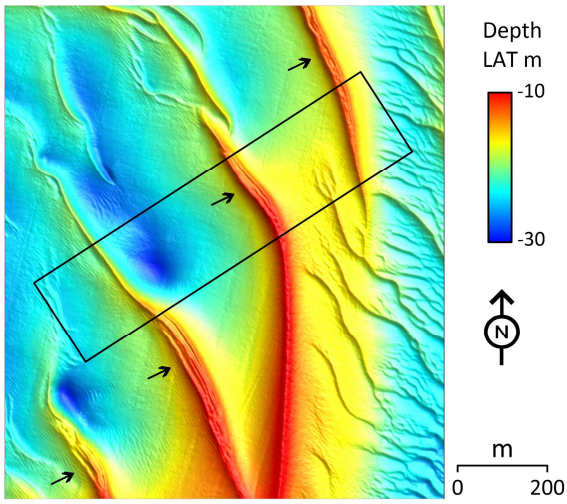

Figure 5. Complex sand wave pattern of the northern end of the Westhinder bank around the WH area. The arrows point to areas of sand waves with multiple ridges. FPS Economy data, RV Belgica survey 2009/03).

On a larger scale, in the northern region at the end of the Westhinder bank, the asymmetry of the sand waves indicates two directions of sediment transport in accordance with flow and the ebb similar to those observed in the central part of the bank. (Deleu et al., 2004).

The tide currents convergence combined with the shelly sediment, produces a complex pattern of sand waves (Fig. 5). Some sand waves locally show several parallel ridges modelling their tops in an undulating surface wide up to 30m locally.

3.1 Correlation analysis

The extraction of BS data in 50x10m buffers around the grab samples allows to quantify the correlations between the BS and the granulometric data. These correlation are presented in table 1.

Table 1: Correlation (Pearson's r) BS mean and std with gravel fractions. Significant value ($p < 0.01$) are in bold.

	mean BS dB in ± [20°-60°]	std BS dB in ± [20°-60°]
> 2mm	**0.86**	**-0.57**
2-4 mm	**0.83**	**-0.55**
4-8 mm	**0.82**	-0.46
8-16 mm	0.42	-0.41
16-32 mm	0.08	-0.14
> 32 mm	0.34	-0.45

The BS shows a significant positive correlation with the percentage of gravel. However, the 2-4 mm and 4-8 mm fractions contribute the most to this correlation. The acoustic wave interacts with the sediment on the scale of its wavelength and the grain sizes of these fractions are close to the wavelength of the acoustic signal used (5 mm at 300 kHz). Beyond 8 mm, the correlations are no longer significant, the BS seems not sensitive to an increase in the coarsest fractions. A similar relationship of BS with sediment grain size has been observed in the Belgian part of the North Sea (Montereale Gavazzi, 2019).

Only BR and TB data are considered to evaluate the trend of BS values with respect to the morphological units because these two areas have similar sand wave characteristics (wavelength, amplitude, asymmetry and migration speed) and comparable surface sediments.

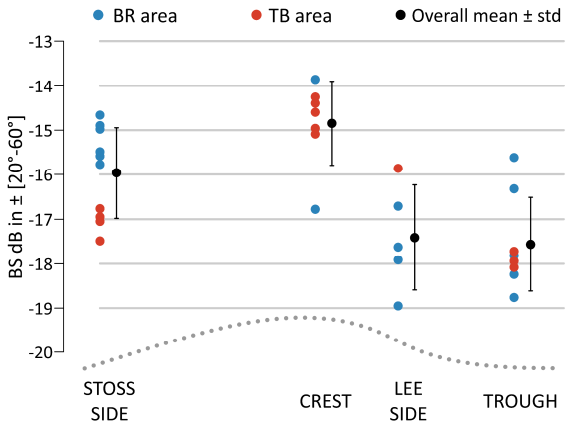

Figure 6. Relationship between BS level and morphological units of sand waves in the BR and TB areas.

The relationships between the mean BS levels estimated in the 50x10m buffers around the grab samples and the morphological units are presented in Fig. 6. Considering BR and TB together, by mean, the BS levels are higher on the stoss sides and the crests than on the lee sides and the troughs but the magnitude of this difference is only 1 to 2 dB.

Within each morphological unit, the range of individual measurements is in the order of 3 to 4 dB, exceeding the range of the overall means values which is 2.5 dB. The variance between the mean BS levels estimated in the buffers surrounding the samples leads to a mixed interpretation.

The pattern is clearer for TB than for BR due to a sharper grain size distribution between the morphological units. In particular, the accumulation of shells and shell fragments on the crests of the sand waves is clearly visible in the SPI images of TB. In BR area, BS levels are more variable within the crests, the lee sides and the troughs. Overall, the SPI images show a more homogeneous seafloor on BR than on TB.

4 CONCLUSION

Careful sample positioning and appropriate corrections to account for the angular dependence of BS are required when coupling MBES bathymetric and high resolution BS data with ground truth data (grab samples and SPI images) to analyse the relationships between surface sediment grain size and sand wave morphology. The use of BS values controlled by the same sediment interface characteristics is ensured by extracting values within a limited angle of incidence range of ±[20°, 60°].

The BS shows a significant positive correlation with the percentage of gravel which consists mainly of shells and shell fragments from 2-8mm close to the wavelength of the acoustic signal used (5 mm at 300 kHz). The spatial relationship between the bathymetry and the BS and the correlations between the BS and the granulometric data demonstrate a granulometric sorting in relation with the sand waves morphological units in line with published data and models.

The peculiar multi-crested shape of the sand waves in an area covered by sediments containing 50% of shells and shell fragments, suggests a sustained control of the sediment on the morphology and dynamics of these sand waves.

In the BR and TB zones, the integration of additional data is necessary to better define the causes of the BS variations in relation to

the morphological units of the sand waves: bathymetric and calibrated BS time series, local hydrodynamic data and granulometric analysis of the sandy fraction.

The dominant role of shells and shell fragments in the acoustic response of the sediment is largely confirmed. However, the field data remain sparse compared to the acoustic data. The addition of field data, including geotechnical ones, is necessary to better understand the sedimentological significance of the BS.

The approach remains surface based. Cores are needed to verify that, according to Walther's Law (Middleton, 1973), the lateral distribution of sediments at the surface of the sand waves is reflected in their vertical sedimentary sequence. However, offshore cores are expensive, so funding must be considered.

5 ACKNOWLEDGMENTS

The VLIZ and the crew of the RV Simon Stevin are acknowledged for providing the ship time, the organization and the good execution of the measurements and collection of samples and images during the campaign 22-600 in October 2022.

6 REFERENCES

APL, 1994. APL-UW High-Frequency Ocean Environmental Acoustic Models Handbook. Technical Report APL-UW TR9407, Applied Physics Laboratory, University of Washington, Seattle, WA, USA.

Anthony, D., Leth, J.O., 2002. Large-scale bedforms, sediment distribution and sand mobility in the eastern North Sea off the Danish west coast. Mar. Geol. 182 (3), 247–263.

Cheng, C. H., Soetaert, K., & Borsje, B.W. (2020). Sediment characteristics over asymmetrical tidal sand waves in the Dutch North Sea. Journal of Marine Science and Engineering, 8(6), 409.

Damveld, J. H., Borsje, B. W., Roos, P. C., & Hulscher, S. J. M. H., 2020. Horizontal and vertical sediment sorting in tidal sand waves: Modeling the finite-amplitude stage. Journal of Geophysical Research: Earth Surface, 125.

Deleu, S., Van Lancker, V., Van den Eynde, D., Moerkerke, G. 2004. Morphodynamic evolution of the kink of an offshore tidal sandbank: the Westhinder Bank (Southern North Sea), Continental Shelf Research, Volume 24, Issue 15, 1587-1610.

Hammerstad, E., 2000. EM Technical Note: Backscattering and Seabed Image Reflectivity. Horten, Norway: Kongsberg Maritime AS. Technical note.

Gaida, T. C., van Dijk, T., A.G.P., Snellen, M., Vermaas, T., Mesdag, C., Simons, D., G., 2020. Monitoring underwater nourishments using multibeam bathymetric and backscatter time series, Coastal Engineering, Volume 158, 103666.

Jackson, D.R., Baird, A.M., Crisp, J.J., Thomson, P.A.G., 1986. High-frequency bottom backscatter measurements in shallow water. J. Acoust. Soc. Am. 80, 1188–1199.

Knaapen, M. A. F. (2005), Sandwave migration predictor based on shape information, J. Geophys. Res., 110.

Lurton, X.; Lamarche, G. (Eds) (2015) Backscatter measurements by seafloor-mapping sonars. Guidelines and Recommendations. 200p.

Middleton, G., 1973. Johannes Walther's Law of Correlation of Facies: Geological Society of America Bulletin, 38: 979-988.

Montereale Gavazzi, G., O., A., 2019. Development of seafloor mapping strategies supporting integrated marine management: application of seafloor backscatter by multibeam echosounders. PhD Thesis, Ghent University, Ghent, Belgium.

Roos, P. C., Hulscher, S. J. M. H., Van der Meer, F. M., Van Dijk, T. A. G. P.,Wientjes, I. G. M., & Van den Berg, J. (2007). Grain size sorting over offshore sandwaves: Observations and modelling. In S. J. M. H. Hulscher & C. M. Dohmen-Janssen (Eds.), RCEM 2007, 5th IAHR symposium on river, coastal and estuarine morphodynamics (pp. 649–656). Enschede: University of Twente.

Van Lancker, V., Jacobs, P., 2000. The dynamical behaviour of shallow marine dunes. In: International Workshop on Marine Sandwave and River Dune Dynamics. University of Lille, France

Van Oyen, T., Blondeaux, P., 2009. Grain sorting effects on the formation of tidal sand waves. J. Fluid Mech. 629, 311–342.

Wemmenhove, T., 2004. Grain size sorting on tidal sandbanks. In: International Workshop on Marine Sandwave and River Dune Dynamics. University of Twente, Enschede, Netherlands.